A DETECTOR FOR HIGH FREQUENCY GRAVITATIONAL EFFECTS BASED ON PARAMETRIC CONVERSION AT 10 GHz

C. E. Reece, P. J. Reiner and A. C. Melissinos
University of Rochester, Rochester, New York 14627

Summary

We have constructed a parametric converter using superconducting cavities operating at 10 GHz. Mechanical displacements $\delta x=10^{-13}$ cm have been measured and it is shown that sensitivity of $\delta x=10^{-21}$ cm can be achieved. Such a detector is suitable for the detection of gravitational effects appearing at a frequency 10-1000 KHz and is sensitive to the direct coupling of the gravitational and electromagnetic fields. Applications to high energy storage rings are discussed.

Introduction

We report preliminary results from a prototype detector suitable for the investigation of the gravitaional effects of a stored beam of high enery particles. The possibility of detecting such effects has been discussed previously[1,2,3] and is only briefly reviewed here.

Consider a particle of mass m and energy $E=\gamma mc^2$ circulating in a storage ring of mean radius R as shown in Fig. 1. A stationary mass M placed at a distance b from the ring will be subject to a tidal impulsive force F_t, which results in an average acceleration

$$\langle a \rangle = \langle \frac{F_t}{M} \rangle = \ell \langle \frac{\partial F}{\partial y} \rangle = \frac{1}{\tau_o} \frac{2NmG}{\gamma\beta cb}(\frac{\ell}{b})[2\gamma^2\beta^2 + 1] \qquad (1)$$

Here ℓ is the length of the detector transverse to the beam, G the gravitational constant; m is the mass of the circulating particles, N the number of particles and τ_o the revolution period; in terms of the circulating current $I=eN/\tau_o$. The impulsive force appears at a frequency $\Omega=c\beta/R$ if the particles are stored in one bunch or at $n\Omega$ if n bunches circulate. If the repetition frequency Ω coincides with a natural mode of the detector, the impulses will excite longitudinal oscillations which reach an equilibrium amplitude

$$\delta\ell_{max} = \langle a \rangle Q_m \frac{1}{\Omega^2} \qquad (2)$$

where Q_m is the loaded mechanical Q-value of the detector at the frequency Ω; equilibrium is attained for $t>Q_m/\Omega$. It was shown in ref. (1) that amplitudes of the order of $\delta\ell_{max}\simeq10^{-21}$ can be achieved at presently planned accelerators such as the FNAL Collider or Isabelle.

There are various possibilities for detecting the small excitations of the detector, given that their frequency is exactly known. We have chosen parametric conversion whereby the mechanical motion gives rise to energy transfer between two narrow states of an electromagnetic cavity operated at $f\simeq10$ GHz (X-band). Such a detector offers the important advantage that it will also respond to the direct coupling of the gravitational field to the electromagnetic field stored in the cavity.[1,4]
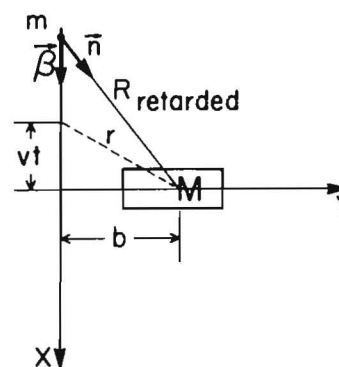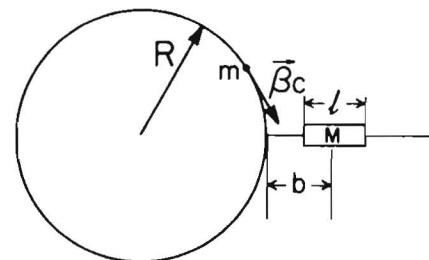
Fig. 1 Arrangement of a massive detector M with respect to a stored beam of high energy particles.

Detector

The detector consists of two identical cylindrical cavities as shown in Fig. 2. The cavities are operated in the TE_{011} mode[5] and coupled through an iris at their common boundary. As a result of the coupling the system possesses two well defined normal modes corresponding to symmetric and antisymmetric field configurations as shown in Fig. 3. The frequency difference between the two modes is given by

$$\Delta f \simeq \sqrt{(f_1 - f_2)^2 + K^2 f_1 f_2} \qquad (3)$$

where the coupling coefficient K depends only on the geometry of the iris; thus Δf can be adjusted to coincide with the frequency Ω of the signal that one wishes to convert. It is clear from Eq. (3) that Δf can be tuned by changing f_1 (or f_2); however only small changes can be made in this way, because the coupling between the two cavities decreases rapidly when $(f_1-f_2)^2 \geq K^2 f_1 f_2$. Power can be fed in or out of the system using coaxial lines with loop terminations as shown in Fig. 2; the amount of coupling to the lines with loop terminations as shown in Fig. 2; the amount of coupling to the lines (i.e. to the outside world) is varied by adjusting the position of the loops within the below cut-off coupling tubes which are mounted on the cavities. A detailed analysis of the e.m. properties of the coupled cavity system has been given by Reece.[6]
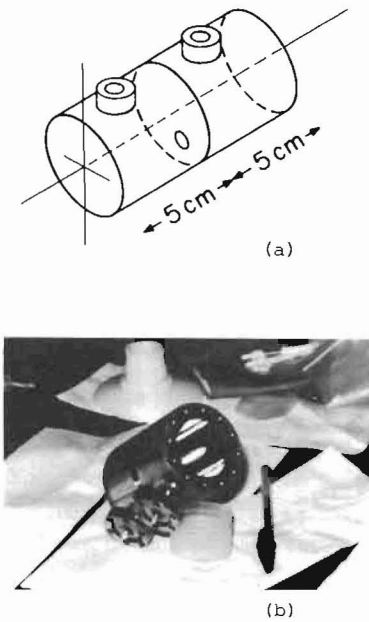
Fig. 2 (a) Sketch of the coupled cavity system
(b) the cavities with the ends removed.
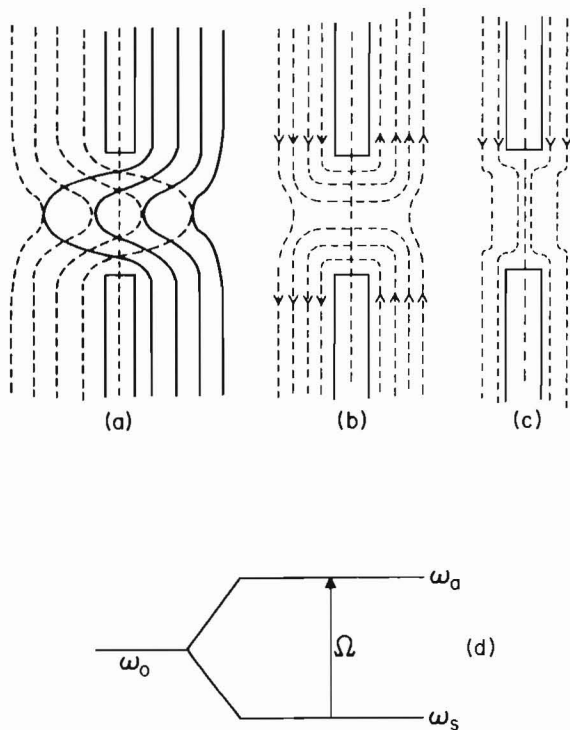
Fig. 3 Magnetic field lines at an iris between two
cavities (a) uncoupled (b) symmetric mode
(c) antisymmetric mode (d) the energy level
diagram after coupling two equivalent cavities.

The cavities are constructed out of Niobium and
operated at liquid Helium temperatures so that they
are superconducting; the cryostat assembly is shown in
Fig. 4. Indium seals were used on the cavity and the
vacuum was 5×10^{-8} Torr. The inner surface of the cavi-
ties was electropolished by the Siemens method and then
oxypolished[7] in order to improve the electrical Q.
Figure 5 shows the measured unloaded Q as a function of

temperature for a particular set of coupled cavities;
the BCS theory prediction[8] for f=10 GHz is shown for
comparison. The observed leveling of the Q for T≲3°K
is probably due to surface conditions and should be
improved by annealing under high vacuum.[9]
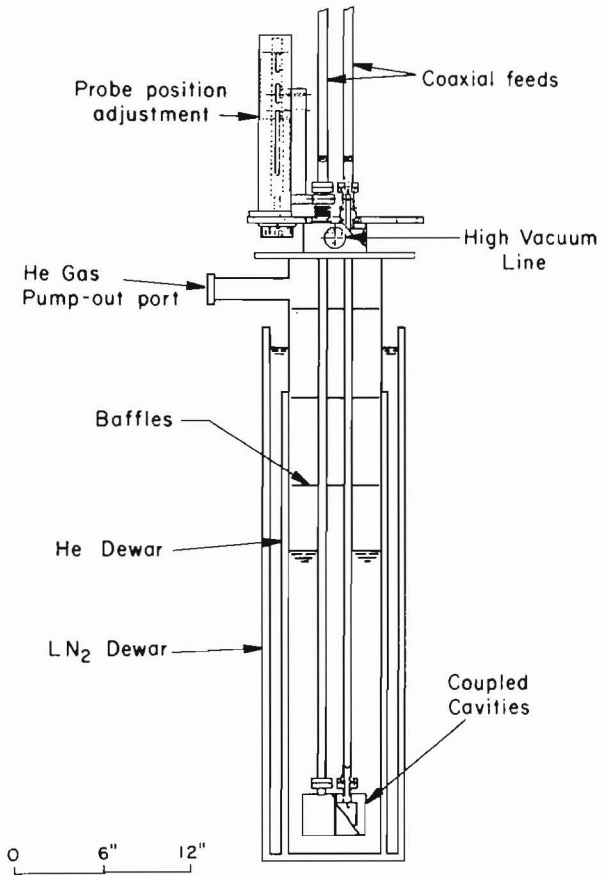
Fig. 4 Assembly drawing of the cryostat.
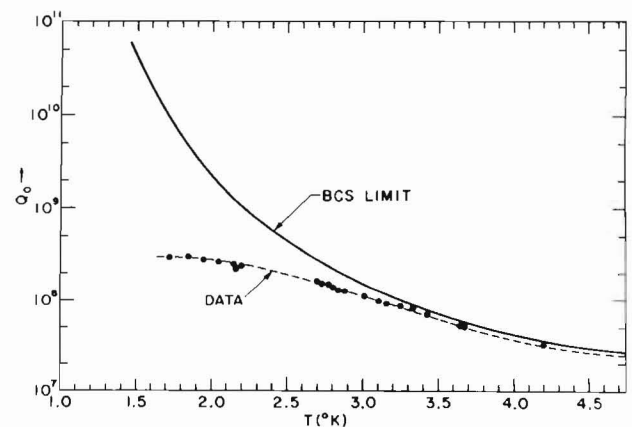
Fig. 5 The unloaded Q of the cavities as a function
of temperature. The solid curve is the BCS
theory prediction from Ref. 8.

To operate the detector as a parametric converter
one of the two normal modes is loaded so that the
energy density in the cavities at frequency f_1 is U_1.
To reach this condition power $P_1^{incident}$ must be sup-
plied at the input port, whereas power P_1^{out} is radi-
ated through the other port,

-395-

$$P_1^{incident} = \frac{U_1 \omega_1}{Q_o} \frac{(1 + \beta_{11} + \beta_{21})^2}{4\beta_{11}} \qquad (4a)$$

$$P_1^{out} = \frac{U_1 \omega_1}{Q_o} \beta_{21} \qquad (4b)$$

In Eqs. (4), β_{ij} are the coupling coefficients for port i and mode j, and Q_o the unloaded Q-value. If a time-dependent perturbation that couples the two modes is now introduced, and if its frequency is near $\Delta f = f_1 - f_2$, transitions will take place between the two modes. In particular energy will be stored in the mode at f_2 and power radiated at the frequency f_2. The rate of energy transferred from mode 1 to mode 2 is[10]

$$\frac{dU_2}{dt} = \frac{\omega_1 t}{2} U_1 \omega_1 \left(\frac{\delta\ell}{\ell}\right)^2 \qquad (5a)$$

The energy U_2 stored in mode 2 reaches its maximum value when dU_2/dt equals the dissipated power $\omega_2 U_2/Q$

$$U_2(max) = U_1 \left(Q \frac{\delta\ell}{\ell}\right)^2 \qquad (5b)$$

and therefore the power radiated at f_2 is

$$P_2^{out} = \frac{U_2 \omega_2}{Q_o} \beta_{22} = P_1^{out} \left(Q \frac{\delta\ell}{\ell}\right)^2 \left(\frac{\omega_2 \beta_{22}}{\omega_1 \beta_{21}}\right) \qquad (5c)$$

In Eqs. (5) $(\delta\ell/\ell)$ is a dimensionless ratio measuring the relative change in the (circuit) <u>parameter</u> giving rise to the frequency conversion.

As an example, motion of the end-walls of the cavity couples the two modes through the absorption of a photon $h\nu_1$ and the subsequent emission of a photon $h\nu_2$ as shown in the graph. We can think of the photons as being absorbed and emitted by the vibrational quanta, phonons, in the wall (this is an analogous process to resonant absorption in the Mössbauer effect). While Eqs. (5) are completely general, in the case of the moving end-walls they can be derived from a simple physical argument, as follows: Assuming that the wall motion is harmonic $X = A\cos\Omega t$, the photons reflected from the wall are Doppler shifted to a frequency

$$f_1' = f_1 (1 \pm v/c) = f_1 \mp f_1 \frac{A\Omega}{c} \sin\Omega t \qquad (6)$$
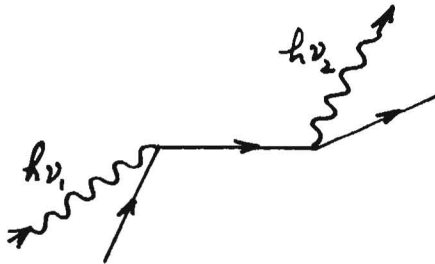
Equation (6) implies frequency modulation of the standing wave and as is well known[11] this gives rise to sidebands at frequencies $f_1 \pm (\Omega/2\pi)$, $f_1 \pm 2(\Omega/2\pi)$,...etc. If one of the sidebands coincides with f_2 then the field at that frequency can be stored in the cavity and eventually reaches the equilibrium value given by Eq. (5b).

Another perturbation which couples the two modes is a periodic change of the total energy stored in the cavity as would arise if the permittivity of the vacuum was modulated. But this is exactly the effect produced by a change in the metric of space induced by a time-dependent gravitational field.[12] In this case Eq. (5c) takes the form

$$P_2^{out} = (hQ)^2 \frac{U_1 \omega_2}{Q_o} \beta_{22} \qquad (5d)$$

where h is dimensionless and measures the deviation of the metric tensor g_{ij} from its flat-space (Minkowski) value η_{ij}

$$g_{ij} = \eta_{ij} + h_{ij}$$

Such detectors were proposed by Pegoraro et al[4] and are further discussed in ref. 13.

An important feature of the detector is that the two normal modes are orthogonal to one another. This manifests itself in that the power radiated at f_1 (the symmetric mode) is in phase at the two ports of the cavity, whereas the power at f_2 is 180° out of phase. This property is used to operate the detector as a balanced bridge by suppressing the loaded mode (at f_1) in the path leading to the detection of the converted power (which appears at f_2). Power suppression factors of 70 db were easily achieved as discussed later (see Fig. 10).

In Table I we list the design parameters for a prototype detector as well as the values already achieved.

TABLE I

Specifications for parametric converter

	Design	Achieved so far
f_0	10 GHz	10 GHz
U_1	1 Joule	10^{-3} J
Q	10^{11}	3×10^8
P_{min} (det)	10^{-22} Watts	10^{-17} W in 1 Hz BW

The above design parameters are realistic and within the limits of present technology. They lead to a minimum value of

$$(\delta\ell/\ell) \quad \text{or} \quad h \simeq 10^{-22}$$

Assuming signal averaging over a time period of 10^6 sec, this limit can be improved to

$$(\delta\ell/\ell) \quad \text{or} \quad h \simeq 10^{-25}$$

The greater sensitivity over other gravitational detectors is due to the knowledge of the perturbing frequency and its stability.

Results

The cavities were excited by a varactor tuned Gunn effect diode oscillator delivering 40 mW at 10 GHz. A Varian VTX-6089P2 travelling wave tube (TWT) amplifier could be used to deliver up to 10 Watts of power. At high Q-values the operating frequency was maintained at the center of the cavity resonance by a phase lock loop system with adjustable gain.[14] Stability of 1 Hz (i.e. 1 part in 10^{10}) is easily realized when $Q \simeq 10^7$ provided the cavity temperature is stable.

The operating configuration can be adjusted to any one of several types of measurement: one such arrangement is shown in Fig. 6. As the simplest illustration of performance we show in Fig. 7 the reflected and transmitted power as a function of frequency; Fig. 7a is at liquid Nitrogen temperature (T=77°K) and Fig. 7b at liquid Helium (T=4.2°K). As the frequency is swept, first mode 1 and then mode 2 are excited. At room

temperature the two modes overlap but when the cavities are superconducting the width of the resonances is reduced by a factor of $\sim10^4$ and the two modes are clearly separated.
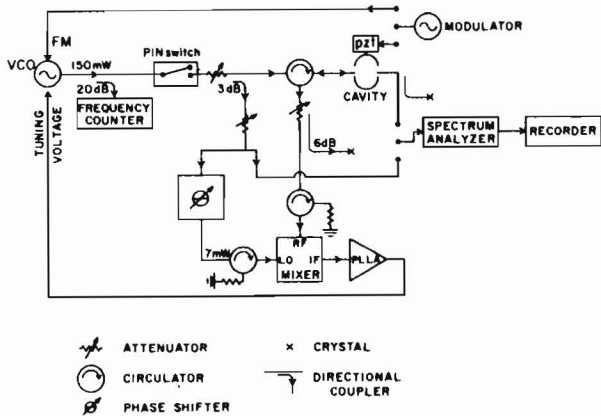
Fig. 6 Schematic of the microwave circuitry.
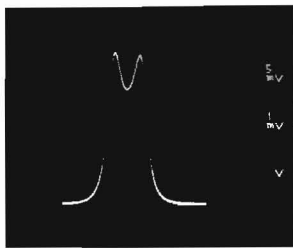
(a)

→| |←698 KHz
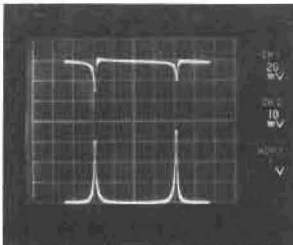
(b)

→|698 KHz|←

Fig. 7 Result of sweeping the frequency across the two normal modes of the system. (a) Transmitted power when the cavities are at T=77°K. (b) Transmitted power (lower trace) and reflected power (upper trace) when the cavities are at T=4.2°K; the peaks in (a) and (b) coincide exactly (the frequency scale has been adjusted).

To make quantitative Q-value measurements a fast switch (a PIN semiconductor device) is used to pulse the microwave power; switching times are typically <30 nsec. In contrast the cavity filling and decay times are much longer as can be seen in Fig. 8a; the upper trace is the reflected and the lower trace the transmitted power. While the transient effects are in general complex and depend on coupling and matching[6], the decay time constant τ_t of the transmitted power is related to the loaded Q of the system to a good approximation through

$$Q_L = \omega\tau_t \qquad (7)$$

By making measurements for different couplings (changing the insertion of the coupling loops[6]) one obtains the results shown in Fig. 9 from which Q_o, the unloaded Q-value, can be deduced. An amusing manifestation of the long decay times can be seen in Fig. 8b where the frequency is swept across the resonance at ~10 kHz/cm. The generator frequency beats against the fixed frequency of the power emanating from the cavity to give rise to the sharp interference pattern; as expected, the beat frequency is proportional to the displacement of the sweep frequency from the resonance value.
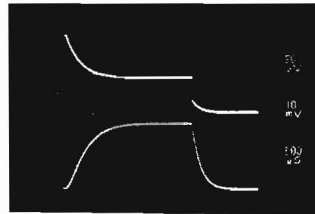
(a)

(b)
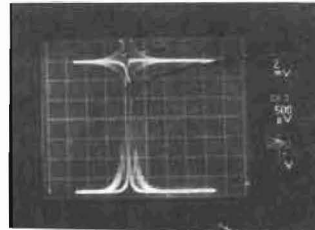
(c)

Fig. 8 (a) Typical data from measuring the Q-value by observing the "ringing" of the cavity: the lower trace shows transmitted power in response to a square wave excitation; the upper curve is reflected power. (b) The tail of the transmitted power for $Q_o \simeq 2.4 \times 10^8$. (c) Beats between the power stored in the cavity at its resonant frequency and an externally swept frequency. The horizontal scale is ~1 msec/cm and, the frequency is swept at the rate of ~10 kHz/cm.

Another diagnostic technique that we used extensively is to modulate (preferably the frequency rather than the amplitude of) the source while the carrier frequency is locked to one of the cavity resonances. This creates sidebands which are, of course, present at the input to the cavity; however the sidebands will not appear at the output unless a sideband frequency coincides with the second mode of the system. This is illustrated in Fig. 10a where the frequency spectrum of the transmitted power is shown on a logarithmic scale as obtained with a HP 8552B spectrum analyzer. The source was frequency modulated at an amplitude $\delta=0.02$ and with $f_m=\Delta f$ equal to the frequency splitting

of the two normal modes. The carrier to sideband power level ratio is

$$\frac{P_s}{P_c} = -34 \ db = (0.02)^2 = \delta^2 \qquad (8)$$

as expected for low modulation amplitudes[15]. Only one of the sidebands is transmitted, the one corresponding to the second normal mode.
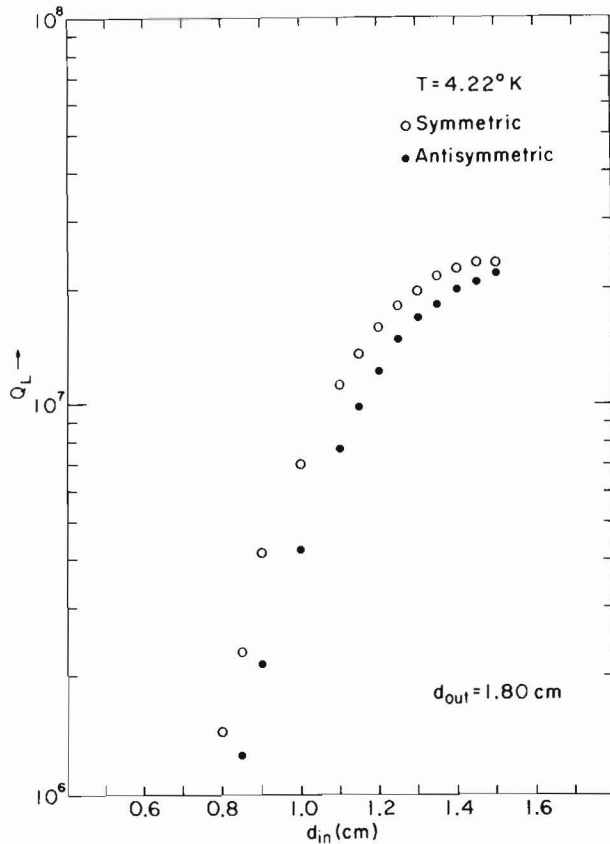
Fig. 9 The measured loaded Q as a function of coupling (probe insertion) for each of the two normal modes. The asymptotic value gives Q_0.

Figure 10b shows the effect of carrier suppression. The transmitted power is now observed through one port of a hybrid which is fed symmetrically by the two cavity ports. By adjusting the phase of the inputs to the hybrid the carrier was suppressed by 70 db as can be seen by comparing Figs. 10a and 10b which were obtained under identical excitation of the cavities.
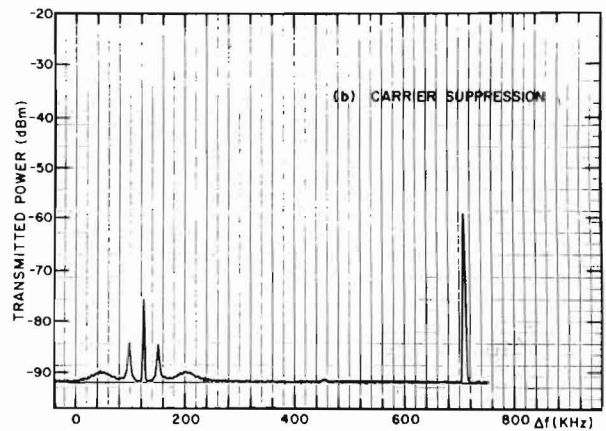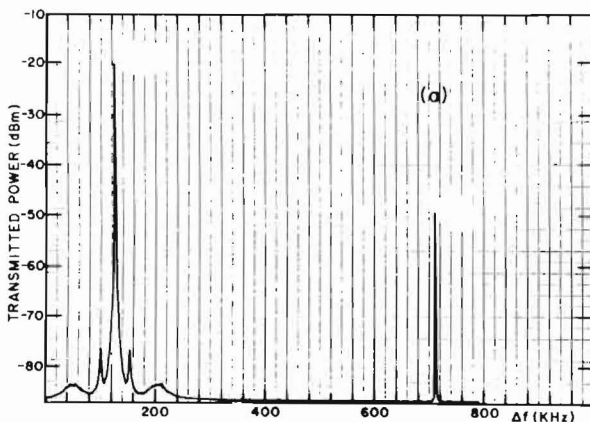
Fig. 10 (a) The frequency spectrum of the transmitted power when the carrier is locked on mode 1 and the source is frequency modulated at $f_m = \Delta f$. The 40 KHz sidebands are produced by the locking (b) same conditions as in (a) but with mode suppression of the carrier. These data were obtained with a spectrum analyzer with 1 MHz bandwidth; the ordinate is a logarithmic power scale.

The power transmitted in the sideband as a function of the modulation frequency, f_m is shown in Fig.11. Such data can be used to assess the rejection of unwanted frequencies and to map out the position and width of the second mode. Since we are sweeping the frequency difference which is 10^4 times smaller than the resonant frequency the resolution is correspondingly improved. The apparent sensitivity limit in Fig. 11 at 10^{-13} watts for $f_m < \Delta f$ is instrumental and due to spectrum analyzer bandwidth and noise as well as to the non-suppression of the carrier. A further advantage of this method is that the appearance of spurious signals (i.e. at the wrong frequency) is an indication of pick-up either through ground loops or through the phase locking loop network. The observed line shape of the carrier (loaded mode) is significantly narrower than the Lorentzian curve calculated from the observed Q of the system; this (desirable) effect is probably due to the phase locking to the center of the resonance curve.

The spectrum analyzer technique allowed us to detect power in the second mode with a sensitivity of $P_{min} \sim 10^{-15}$ watts in a bandwidth $\Delta \nu \approx 100$ Hz, and with $P_{carrier} = 10^{-4}$ watts maximum. To achieve better sensitivity we must select and isolate the power in the second mode. This is achieved by mixing the transmitted signal with the carrier in a double-balanced microwave mixer. If power is present at f_2 the mixer output will contain an intermediate frequency (IF) at Δf (Δf is the splitting of the two normal modes). This IF is amplified and then selected by using a lock-in-amplifier which is referenced by the generator of the perturbation. A schematic of the detection scheme is shown in Fig. 12. In the tests reported here the carrier was not suppressed, and this increased the mixer noise as well as limiting the power that could be loaded in the first mode. The results shown in the right-hand-side column of Table I were obtained under these conditions.
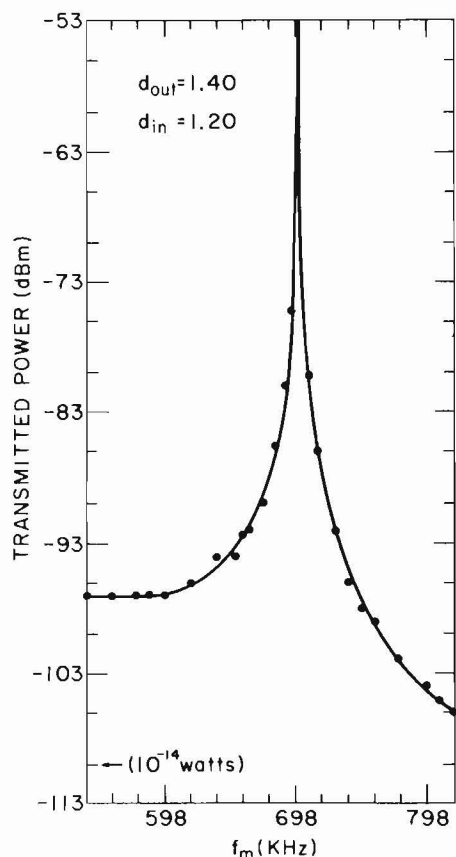
Fig. 11 The transmitted power in the sideband as a function of the modulation frequency f_m. The data can be approximated by a Lorentzian with Q-value $\sim 1.2 \times 10^7$. The carrier is located toward the ℓ.h.s. of the abscissa and has a peak value of -20 dbm; the carrier line is significantly narrower than the natural width of the cavity (exhibited by the sideband).
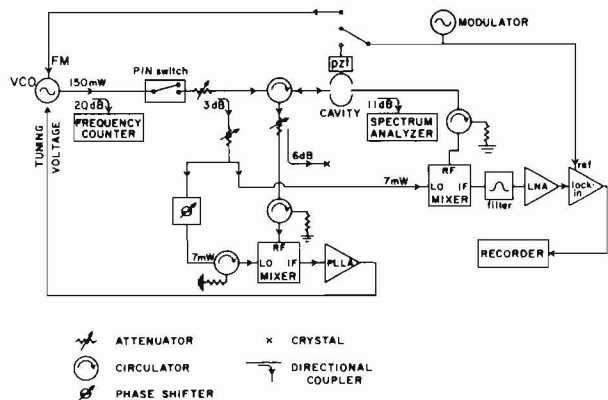
Fig. 12 Schematic (as in Fig. 6) but showing the demodulation mixer, low-noise-amplifier and lock-in detector elements.

To demonstrate parametric conversion piezoelectric crystal transducers (pzt) were attached to the end walls of the cavity; the best transfer of power was obtained by using Nonag Stopcock grease (from Fisher Scientivid Co.) which maintained its bond in liquid helium. The nominal displacement of a free pzt is given as $\delta x = 2.5 \times 10^{-8}$ cm per 1 volt peak-to-peak. However the spectrum of mechanical vibrations of the

cavity at the frequency of interst, $\Delta f \sim 700$ kHz is very complex and the resonances correspond to high harmonics; it is almost a continuum. This can be seen in Fig. 13 which shows the pick-up signal from a pzt mounted on one end-wall when the other wall is driven by a similar pzt. The frequency spectrum was obtained with the lock-in amplifier and one can recognize the expected correlation between the quadrature and in-phase signals. While the pzt have their own spectral response the structure indicated by Fig. 13 is principally due to the mechanical properties of the cavity; this structure is highly reproducible and dominant lines can be identified under a variety of conditions. At present we do not know how to calculate the actual displacement of the walls under the influence of the pzt's and at a particular frequency; furthermore the displacement depends on the mechanical coupling. A hand-waving estimate is

$$\delta \ell \sim \frac{\delta x}{Q_m} \sim 5 \times 10^{-12} \text{ cm/volt} \tag{9}$$

to which we attach an uncertainty of a factor of 10 either way.
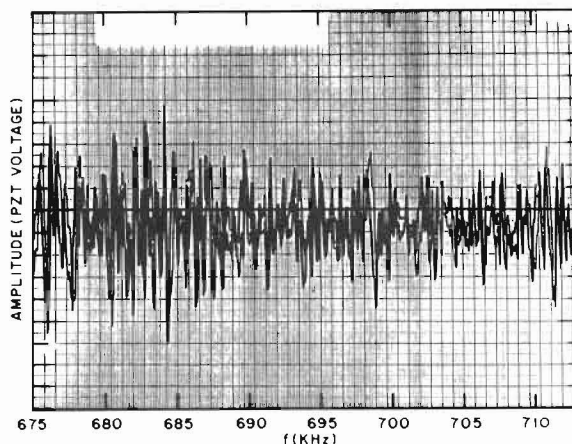
Fig. 13 In-phase and quadrature signal response of a pzt mounted on one end-wall of the cavity when the other wall is driven by a pzt with 10V excitation. The frequency range spanned is 715 kHz and shows the spectrum of mechanical resonances that are excited. Typical widths are $\Delta f/f \sim 10^{-3}$.

A typical result of power converted to the frequency f_2 under the influence of pzt excitation of the cavity end-wall is shown in Fig. 14. The in-phase and quadrature signals from the lock-in amplifier are recorded as a function of the pzt frequency (upper trace). To indicate the position of the second mode the same signals (but with power gain reduced by 60 db) are displayed in the lower trace in response to frequency modulation of the source. In both cases the lock-in reference was obtained from the signal driving the pzt, or generating the FM. Parametric conversion occurs at the electrical resonant frequency provided the amplitude of cavity wall motion is significant as is the case only when a mechanical resonance is crossed. The envelope of the converted signal matches the electrical Q of the cavity, as indicated by the dashed curve. The relation between the in-phase and quadrature components of the signal is a further indication that genuine resonances occur at certain frequencies. Similar results have been obtained with the spectrum analyzer.
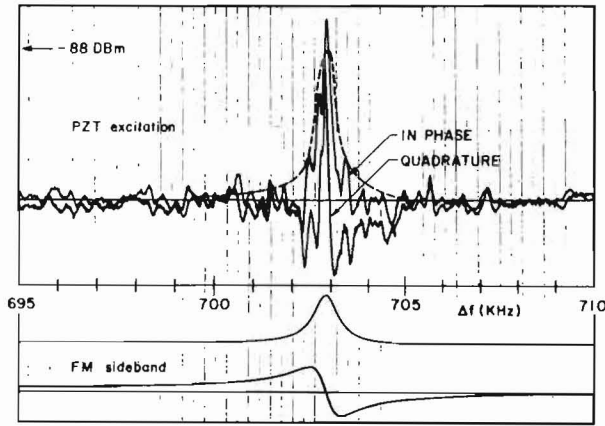
Fig. 14 Evidence for parametric conversion. The upper trace is the response to 10V pzt excitation as a function of frequency. The lower curve is obtained by frequency modulating the source and locates the position and width of the second state; it is overlayed on the upper trace as a dashed curve. The integration time was 0.1 sec and the peak signal $\sim$ −88 dbm of IF; the data were taken at T= 2.25 °K and $Q_L \approx 1.4 \times 10^7$.

The power in the converted mode depends quadratically on the amplitude of the end-wall motion; this relation is verified experimentally by the data of Fig. 15 where the signal from the lock-in amplifier is plotted vs. the voltage applied to the pzt. According to Eq. (5c) these two variables should be related linearly[16] as observed for the data. The smallest power level that could be separated from the noise (without signal averaging) was P=−67 dbm as observed on the lock-in for a bandwidth $\Delta\nu$=1 Hz. The LNA (low noise amplifier) had a power gain of 60 db and the loss in the microwave mixer was 7 db so that the observed signal corresponds to

$$P_{min} = -120 \text{ dbm} = 10^{-15} \text{ Watts} \qquad (10)$$

without taking account of losses in the lines. This result is of the same sensitivity as obtained with the spectrum analyzer but should be improved in the future. We note for reference that the power stored in the cavity at the carrier frequency was only

$$U_1 \simeq 3 \times 10^{-7} \text{ J} \qquad (10')$$

The amplitude of wall displacement is directly related to the ratio of the output power at the two modes as shown in Eq. (5c): to a good approximation we can write

$$\frac{P_2^{out}}{P_1^{out}} = \left(Q_L \, \frac{\delta\ell}{\ell}\right)^2 \qquad (11)$$

where Q_L, the loaded Q-value depends on the coupling and the temperature. As a consequence the converted power depends on these variables in a complex fashion. In Table II we give results obtained under varying conditions from which we can extract $\delta\ell/\ell$; Δf_c and Q_L are measured experimentally by using the frequency modulation technique. While there is some dispersion in the results the average value is

$$\frac{\delta\ell}{\ell} \simeq 1.3 \times 10^{-12} \text{ cm/volt (pzt)}$$

or using $\ell \simeq 4$ cm

$$\delta\ell \simeq 6 \times 10^{-12} \text{ cm/volt (pzt)} \qquad (11')$$
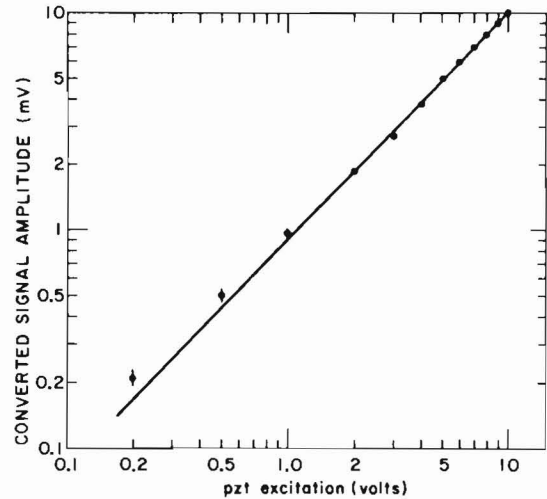
Fig. 15 Converted voltage signal as a function of exciting pzt voltage. Note the almost linear relation between these voltages as predicted by Eqs. (5) of the text.

If the actual wall displacement was known the above result could be used to verify the derivation of Eq. (11). However, given the uncertainty in the estimate presented in Eq. (9) the agreement must be considered fortuitous.

The ultimate sensitivity obtained with the present system was of the order of P_2^{out}/P_1^{out}=−120 db and pzt excitations of 0.1 volt. This corresponds to harmonic motion of amplitude

$$\delta\ell_{min} \sim 3 \times 10^{-13} \text{ cm (achieved)} \qquad (12a)$$

We expect to improve the Q-value to 10^{11} (factor of $\sim 5 \times 10^3$) the carrier power to 0.1 watt (factor of 10^2) and the detection sensitivity to 10^{-22} watt (factor of 10^7). Since $\delta\ell$ is proportional to the square root of the power ratios the overall improvement factor is $\sim 1.5 \times 10^8$ leading to

$$\delta\ell_{min} \simeq 2 \times 10^{-21} \text{ cm (expected)} \qquad (12b)$$

The expected sensitivity is to be compared with the thermal motion (at T=2.2 °K) of a mechanically _untuned_ detector where[13]

$$\delta x = 3.6 \times 10^{-22} \text{ cm}$$

On the other hand for a mechanically tuned detector one has the much larger thermal motion amplitude of

$$\delta x \simeq 10^{-16} \text{ cm}$$

so that thermal noise contributions may appear before reaching the limit shown in Eq. (12b). Signal averaging should provide further discrimination against random noise.

TABLE II

Results from Parametric Conversion Under Varying Conditions

Temperature (^{o}K)	4.2	4.2	2.3	2.4	2.4
Coupling[a] d_{out}	1.10	0.90	1.10	1.20	1.20
d_{in}	1.40	1.10	1.40	1.10	1.10
Δf_c (kHz)	701.4	697.57	701.48	703.35	703.35
Q_L	1.7×10^7	0.52×10^7	2.2×10^7	1.3×10^7	1.3×10^7
V_{pzt} (volts)	10	10	10	10	1
P_1^{out} (dbm)	-13	0	-6	-5	-5
P_2^{out} (dbm)	-84.4	-88	-77	-80	-100
$\delta\ell/\ell$	1.6×10^{-11}	7.7×10^{-12}	1.3×10^{-11}	1.3×10^{-11}	1.3×10^{-12}

(a) Entries in the table measure the insertion of the loops in cm; smaller values of d imply stronger coupling.

Possible Applications at High Energy Storage Rings

As mentioned in the introduction if a resonant detector is placed in close proximity to the circulating beam it will respond to the periodic impulses. For a distance b=10 cm and $N=10^{15}$ particles (!!) at E= 1000 GeV the amplitude of the mechanical oscillations reaches[1] $\delta x \approx 10^{-21}$ cm provided the mechanical $Q_m \approx 10^9$. This is in principle measurable (see Eq. (12b)) but since the detector is tuned the thermal noise may mask the effect.

For an untuned detector one would exploit the direct coupling of the gravitational field to the e.m. field in the cavity. Under the same conditions as above the peak value of the change in metric $h \approx 10^{-31}$ and occurs when the bunch is at the distance of closest approach[1,13]. This value of h is still smaller by a factor of 10^6 than the minimum detectable power as previously given. Furthermore if the periodic impulses are Fourier analyzed, the basic frequency component Ω appears with an amplitude in h which is

$$\tilde{h} \simeq <h> \simeq 10^{-38} \qquad (13)$$

namely a further reduction by a factor of 10^7. Operating the detector in close proximity to the beam poses serious problems because of the e.m. background and particle background which appear at the same frequency. The e.m. effects will be suppressed because of the presence of the superconducting material; particle interactions in the detector can be minimized by appropriate placement of the detector. Nevertheless the gravitational effect is so small that it is important to measure these background effects experimentally, in order to establish the lowest sensitivity level.

If one considers only the direct coupling then a natural location for the detector is at the center of the ring. In this case the components of h rotate in synchronism with the bunches and their magnitude is given by Eq. (13). However, background effects are practically eliminated since the electromagnetic fields are attenuated by $\sim$1000 m of earth. It can be shown[13] that the rotating gravitational field induces transitions between the two modes of the detector so that the power radiated at f_2 reaches the equilibrium value predicted by Eq. (5d). The stability of the circulating frequency of high energy accelerators is of the order of 1 part in 10^7–10^8 which matches a $Q \sim 10^{11}$ at the natural modes of the detector f_0; recall that $\Delta f \sim 10^{-4} f_0$.

Observation of the gravitational effect of a circulating beam of high energy particles would provide a laboratory test of general relativity. In many respects the experiment is the complement of the bending of light where, as in the present case, the general and special relativity results differ by a factor of 2. More importantly however the energy dependence of the bending of the trajectory of a massive particle is a direct measure of the spin of the graviton: the effect depends on the energy as E^{s-1} where s is the spin of the quantum carrying the interaction. This dependence can be used to separate residual electromagnetic effects, and to probe for an s=0 contribution to the propagation of gravitational fields.

In conclusion it appears that the gravitational effect of presently planned storage rings is at the limit of sensitivity of mechanically tuned detectors whose motion can be detected by parametric conversion. Thermal noise and environmental background must be studied further. On the other hand parametric converters exploiting the direct coupling of the gravitational and e.m. fields can be used at present high energy storage rings to search for gravitational effects that are several orders of magnitude larger than predicted by general relativity. We have constructed such a detector and believe that it is important to further improve their sensitivity and to test their operation in an accelerator environment.

References and Notes

1. A. C. Melissinos, Il Nuovo Cimento 62B, 190 (1981).
2. V. B. Braginsky, C. M. Caves and K. S. Thorne, Phys. Rev. D15, 2047 (1977).
3. C. E. Reece, A. C. Melissinos and P. J. Reiner, "A possible test of general relativity at Isabelle," in Proceedings of the 1981 ISABELLE Workshop, p.592. BNL Report 51443.

4. F. Pegoraro, E. Picasso and L. A. Radicati, J. Phys. $\underline{A11}$, 1949 (1978); F. Pegoraro, L. A. Radicati, Ph. Bernard and E. Picasso, Phys. Lett. $\underline{A68}$, 165 (1978); C. M. Caves, Phys. Lett. $\underline{B80}$, 323 (1979).

5. The TM_{111} mode which is degenerate to the TE_{011} was suppressed by machining a groove at the end of the cavities.

6. C. E. Reece "Properties of Coupled Microwave Cavities," University of Rochester report UR-791 (unpublished).

7. P. J. Reiner "Preparation Techniques for High Q Superconducting Cavities" University of Rochester report UR-807 (unpublished); see also Diepers, Schmidt, Martens and Sun, Phys. Letts. $\underline{37A}$, 139 (1971).

8. The BCS theory prediction is from J. P. Turneaure and I. Weissman, Jr. of Applied Physics $\underline{39}$, 4417 (1968).

9. See, for instance, M. Strongin, C. Varmazis and A. Joshi, in "Treatise on Materials Science and Technology" $\underline{Vol.\ 14}$, p. 327 (1979) published by Academic Press, N.Y. Also H. J. Halama, Particle Accelerators (Gordon and Breach) $\underline{2}$, 335 (1971).

10. The linear dependence of dU_2/dt on t is due to the fact that the rate of energy transfer is proportional to the energy already stored in mode 2.

11. See for instance, C. P. Poole, "Electron Spin Resonance" p. 458, Interscience, N.Y. (1967) or S. Seely "Electron Tube Circuits" McGraw Hill, N.Y. (1950).

12. See, for instance, L.D. Landau and E. M. Lifshitz, "The Classical Theory of Fields," Pergamon Press, 4th edition (1975).

13. "Working notes on gravitational effects of stored beams of high energy particles," compiled by A. C. Melissinos, University of Rochester internal report (unpublished).

14. We thank the Cornell superconducting RF group for the design of the circuits and in particular R. Sundelin, D. Rice and K. Krafft.

15. See Refs. (11, 13). For our source a 1 V bias on the varactor produces a frequency shift $\Delta\omega \simeq 1$ MHz. The modulation amplitude δ is defined through $\omega_m \delta = \Delta\omega$ so that for 75 mV bias and $\omega_m \simeq 750$ kHz, $\delta \simeq 0.1$.

16. The wall motion $\delta\ell$ is linear in pzt voltage and therefore the converted power is quadratic in pzt voltage; on the other hand the converted power is given by the square of the lock-in voltage signal.